Synthetic Communications
An International Journal for Rapid Communication of Synthetic Organic Chemistry
ISSN: 0039-7911 (Print) 1532-2432 (Online) Journal homepage: www.tandfonline.com/journals/lsyc20

Microwave-driven synthesis of α-aminophosphonates targeting diabetes: *in silico* and *in vitro* assessment of *α*-amylase and *α*-glucosidase inhibition

Manjula K. , Raja Rajeswari T. & Subramanyam Ch.

To cite this article: Manjula K. , Raja Rajeswari T. & Subramanyam Ch. (02 Dec 2025): Microwave-driven synthesis of α-aminophosphonates targeting diabetes: *in silico* and *in vitro* assessment of *α*-amylase and *α*-glucosidase inhibition, Synthetic Communications, DOI: 10.1080/00397911.2025.2592258

To link to this article: https://doi.org/10.1080/00397911.2025.2592258

SYNTHETIC COMMUNICATIONS®
https://doi.org/10.1080/00397911.2025.2592258

Microwave-driven synthesis of α-aminophosphonates targeting diabetes: *in silico* and *in vitro* assessment of *α*-amylase and *α*-glucosidase inhibition

Manjula K.[a], Raja Rajeswari T.[b] and Subramanyam Ch.[c]

[a]Department of Chemistry, Rajiv Gandhi University of Knowledge Technologies, APIIIT, Srikakulam, India; [b]Department of Chemistry, Sri A.S.N.M. Government College (Autonomous), Palakol, India; [c]Department of Chemistry (recognized as research centre by A.N. University), Bapatla Engineering College (Autonomous), Bapatla, India

ABSTRACT

A new library of α-aminophosphonate derivatives (**9a–j**) was developed utilizing a Kabachnik–Fields multicomponent method with microwave assistance. Prior to synthesis, their pharmacokinetic characteristics and inhibitory interactions with the enzymes α-amylase and α-glucosidase were predicted using molecular docking simulations and in silico ADMET evaluation. Spectroscopy was used to check the structural integrity. The synthesized compounds were examined in vitro for inhibitory effects against two enzymes associated with type 2 diabetes. Compound **9e** inhibited α-glucosidase the most (IC_{50}=88.89 µg/mL), while compound **9b** inhibited both enzymes (IC_{50}=2.6 µg/mL for α-glucosidase and 102.36 µg/mL for α-amylase), similar to acarbose. SAR analysis found that electron-donating and heterocyclic groups increased activity, whereas bulky or electron-withdrawing substituents reduced efficacy. Statistical validation with ANOVA and Tukey's HSD test revealed significant variations in enzyme inhibition across the compound set. These findings suggest that the synthesized compounds serve as promising candidates for the development of dual-action anti-diabetic agents.

ARTICLE HISTORY
Received 27 June 2025

KEYWORDS
Kabachnik-Fields (K-F) reaction; α-aminophosphonates; microwave irradiation; molecular docking; α-amylase; α-glucosidase

GRAPHICAL ABSTRACT

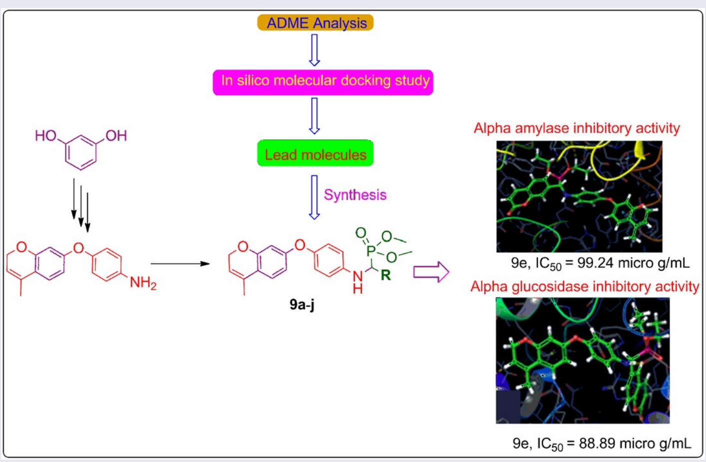

CONTACT Raja Rajeswari T. rajarajeswarit865@gmail.com Department of Chemistry, Sri A.S.N.M. Government College (Autonomous), Palakol, West Godavari (Dt) 534260, India.
Supplemental data for this article can be accessed online at https://doi.org/10.1080/00397911.2025.2592258.

1. Introduction

Diabetes mellitus is a chronic metabolic condition defined by insufficient insulin release from the pancreas or poor cellular responsiveness to insulin production. Sulfonylureas, thiazolidinediones, biguanides, meglitinides, sodium-glucose cotransporter-2 (SGLT2) inhibitors, dipeptidyl peptidase-4 (DPP-4) inhibitors, and glucagon-like peptide-1 (GLP-1) receptor agonists are all commonly used to treat type 2 diabetes mellitus (T2DM) (Figure 1). Inhibiting α-amylase (EC 3.2.1.1) and α-glucosidase (EC 3.2.1.20) is an alternate therapeutic method for slowing glucose absorption.[1–5] Salivary α-amylase begins carbohydrate digestion by cleaving α-(1,4)-glycosidic bonds in starch and similar polysaccharides. This results in shorter glucan chains that are then digested into simple sugars.

When this enzyme activity enters the stomach's acidic environment, it stops, but pancreatic α-amylase action causes it to continue in the small intestine. By cleaving α-(1,4)-glycosidic bonds and, to a lesser extent, α-(1,6)-glycosidic bonds, α-glucosidase aids in the ultimate breakdown of oligosaccharides at the intestinal brush boundary, releasing glucose and other simple sugars. Thus, glycemic management in type 2 diabetes can be supported by inhibiting both α-amylase and α-glucosidase, which can significantly lower postprandial glucose rise.[6] While acarbose and other α-glucosidase inhibitors are employed in clinical settings, they also inhibit α-amylase, as well as other enzymes such sucrase, glucoamylase, maltase, and isomaltase.[7–9] Despite its efficacy, acarbose is commonly associated with gastrointestinal discomfort, such as flatulence, bloating, and diarrhea, because of the buildup of undigested carbohydrates in the colon,[10–13] and it typically necessitates the co-administration of carbohydrates to reduce the risk of hypoglycemia. Finding new, safer, and more effective inhibitors-including both natural and synthetic derivatives-has thus been the subject of intense research.[14–17]

Because of their diverse range of chemical, biological, and physical properties, organophosphorus compounds are widely recognized for their importance in synthetic organic chemistry, agriculture, industry, and medicine.[18–21] Among these, α-aminophosphonates (α-Aps) have garnered significant interest because of their

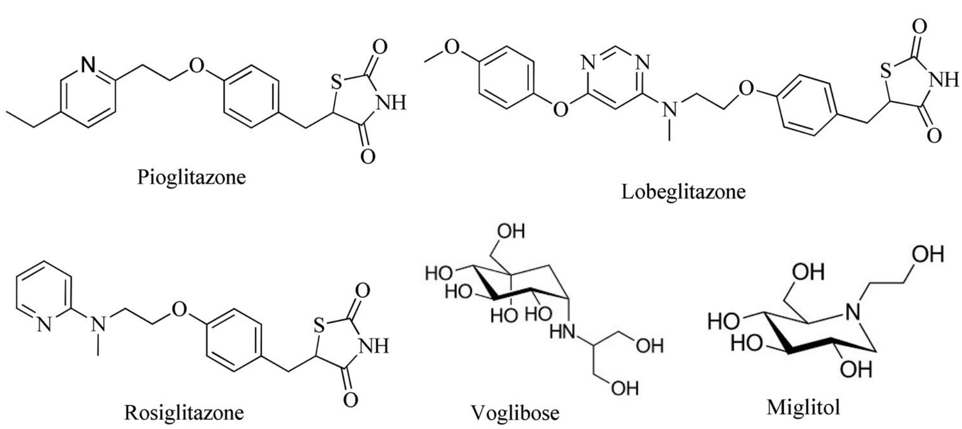

Figure 1. Some known anti-diabetic drugs.

structural similarities to natural amino acids and transition states of peptide hydrolysis.[22] These substances have shown a variety of applications in biological systems,[23] industrial processes,[24] and medicinal settings.[23,25] Potential applications for α-Aps include cancer treatment,[26] antitumor therapies[27,28] anti-inflammatory formulations,[29,30] antibiotics,[31,32] herbicides,[33] fungicides,[34] bactericides,[35] enzyme inhibitors,[36] plant growth regulators,[37] antioxidants,[38] protease inhibitors,[39] metal corrosion inhibitors,[40] antiviral medications,[41] and antidiabetic treatments.[42,43] The synthesis of α-Aps with heterocyclic units, which have demonstrated increased biological activity, has been the focus of recent developments.[44–47] It has been discovered that adding heterocyclic structures to α-Aps frameworks greatly increases their pharmacological potency. The Kabachnik-Fields (K-F) reaction, which involves the nucleophilic addition of phosphites to imines, has been identified as one of the most effective synthetic pathways for the synthesis of α-Aps.[48]

A novel method of activating chemical reactions by supplying energy directly to the molecules of the reactants is microwave (MW) irradiation. Faster reaction rates, higher yields, more pure products, simple processes, and effective synthesis of bioactive heterocyclic compounds are all results of this direct energy transfer, which also speeds up molecular motion.[47,48]

In addition to traditional experimental methods, *in silico* methodologies have become essential in today's drug discovery and development process. With the use of these computational techniques, scientists may more precisely investigate structure–activity connections, identify important chemical interactions, and predict the binding affinities of small compounds to target proteins. Potential inhibitors' binding modalities and interaction mechanisms with particular biological targets can be better understood through the use of molecular docking, molecular dynamics simulations, and related computational techniques. The logical design, structural improvement, and optimization of innovative treatment candidates are made easier by this understanding. Furthermore, by identifying compounds with beneficial interaction patterns, directing synthetic approaches, and reducing the number of candidates for further biological assessment, *in silico* investigations are essential for expediting the drug development process. By eliminating the need for a great deal of trial-and-error testing, this integrated strategy not only speeds up the discovery process but also saves a substantial amount of time, money, and laboratory resources.[49]

Organophosphorus compounds with heterocyclic moieties have been shown in recent studies to have potent inhibitory effect against α-amylase and α-glucosidase, making them attractive options for the treatment of diabetes.[50–59] The goal of this study is to produce a new microwave-assisted synthetic method for making α-aminophosphonates[30,32,60,61] and evaluate how well they block the enzymes α-amylase and α-glucosidase. Furthermore, in vitro tests were carried out to examine the possible antidiabetic action of the synthetic compounds.

2. Results and discussion

2.1. Chemistry

We produced a series of new α-aminophosphonate derivatives (**9a–j**) to inhibit α-amylase and α-glucosidase using in silico molecular docking and ADMET analysis. Compounds

Table 1. MW-assisted synthesis of α-aminophosphonates **9a**–**j**.

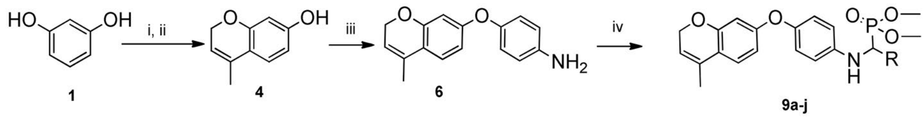

i). Ethyl acetoacetate (**2**), H_2SO_4, 100-120°C, 3h; ii). **3**, $LiAlH_4$, THF, N_2 atmosphere, room temp,, 3h iii). 4-Chloaniline (**5**), THF,TMG, 5-10 ^{O}C; iv) MW (450W), R-CHO (**7a-j**), diethyl phosphite (**8**), 8-15 minutes.

Compound	**9a**	**9b**	**9c**	**9d**	**9e**
R group	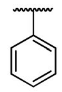	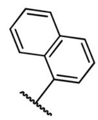	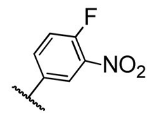	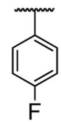	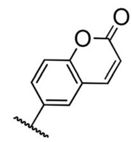
Compound	**9f**	**9g**	**9h**	**9i**	**9j**
R group	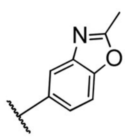	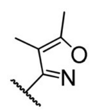	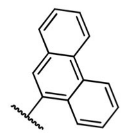	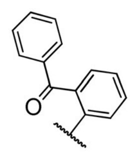	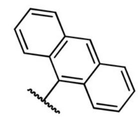

with good docking scores were then synthesized using microwave-assisted, solvent-free conditions, resulting in excellent yields (93%–96%). Table 1 depicts the synthesis approach for *α*-aminophosphonates (**9a**–**j**).

First, benzaldehyde (**7a**), dimethyl phosphite (**8**), and 4-((4-methyl-2*H*-chromen-7-yl) oxy)aniline (**6**) were used in a model process. At the beginning of the investigation, tetrahydrofuran (THF) was used as the solvent and no catalyst was used, and the reaction was conducted at reflux temperature. A low yield (40%) of the product, **9a**, was produced after 24 hours (Table 2, entry 1). After then, the reaction was conducted with 1.2 equivalents of triethylamine present. A yield of 49% was achieved (Table 2, entry 2). A catalyst was then used to carry out the reaction. The model reaction was conducted with catalysts (5 mol%) such as $LaCl_3$, $AlCl_3$, $FeCl_3$, MnO_2, $NiBr_2$, $ZnCl_2$, TiO_2, $CuCl_2$, $ZnBr_2$, and ZnO in an effort to find an effective catalyst (Entries 3–12 in Table 2).

After 6–12 h, the yield of product **9a** rose from 66–80%, suggesting that the catalyst is crucial to this process. Because of its low toxicity, vast surface area, affordability, and environmental advantages, nano-ZnO is becoming more and more popular as a heterogeneous catalyst, according to recent research. The model reaction was then conducted using nano-ZnO as a catalyst. Within one hour, a considerable yield (85%) of the product was produced (Table 2, Entry 13).

On the other hand, microwave radiation speeds up the rate of reactions, which lowers reaction times and increases product yield while minimizing the production of by-products. Therefore, the reaction was conducted utilizing MW irradiation at 400 W

Table 2. MW-assisted synthesis of compound **9a** and optimization of reaction conditions.[a,b]

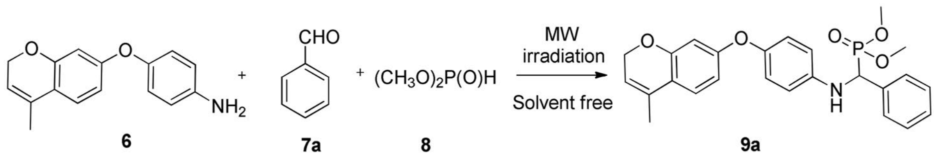

Entry	Catalyst (mol%)	Solvent	Temp. (°C)	Time	Yield[b] (%)
1	–	THF	reflux temperature	24 h	40
2	Et_3N (1.2 eq.)	THF	reflux temperature	10 h	49
3	$LaCl_3$ (5)	THF	reflux temperature	10 h	75
4	$AlCl_3$ (5)	THF	reflux temperature	10 h	73
5	$FeCl_3$ (5)	THF	reflux temperature	10 h	69
6	MnO_2 (5)	THF	reflux temperature	10 h	66
7	$NiBr_2$ (5)	THF	reflux temperature	10 h	77
8	$ZnCl_2$ (5)	THF	reflux temperature	7 h	77
9	TiO_2 (5)	THF	reflux temperature	10 h	75
10	$CuCl_2$ (5)	THF	reflux temperature	10 h	72
11	$ZnBr_2$ (5)	THF	reflux temperature	7 h	79
12	ZnO (5)	THF	reflux temperature	5 h	80
13	Nano-ZnO (5)	THF	reflux temperature	1 h	85
14	–	Solvent-free, MW irradiation	Room temperature	8 minutes	89

[a]Reaction between 4-((4-methyl-2*H*-chromen-7-yl)oxy)aniline (**6**) and benzaldehyde (**7a**) and dimethylphosphite (**8**) was selected as model to optimize conditions of reaction.
[b]Isolated yield.

Table 3. Effect of MW oven power (Watt) on the yield of the compound **9a**.[a]

Entry	Microwave power (Watts)	Yield[b]
1	150	70
2	200	73
3	250	75
4	300	77
5	350	85
6	400	89
7	450	95
8	500	95

[a]Reaction of 4-((4-methyl-2H-chromen-7-yl)oxy)aniline (**6**), benzaldehyde (**7a**) and dimethyl phosphite (**8**) without solvent under microwave irradiation at optimum temperature.
[b]Isolated yield.

without a catalyst in a solvent-free environment in order to further optimize the reaction conditions. Within 8 minutes, a good yield (89%) of the product was produced (Table 2, Entry 14).

We thoroughly examined the impact of microwave power on the model reaction between 4-((4-methyl-2*H*-chromen-7-yl)oxy)aniline (**6**), benzaldehyde (**7a**), and dimethyl phosphite (**8**) in order to maximize the efficiency of the chromene-based bisphosphonate synthesis. Under controlled microwave irradiation, the reactions were conducted without the use of solvents and with applied power ranging from 150 to 500 watts (Table 3). The findings clearly showed that the product yield was significantly impacted by microwave power. The reaction occurred slowly at the lowest power of 150 W (Entry 1), yielding only 70% of compound **9a**. The yield improved gradually when the power was increased: 73% at 200 W (Entry 2), 75% at 250 W (Entry 3), and 77%

Table 4. MW mediated synthesis of **9a–j**.[a]

Structure	Time (min)	Yield[b] (%)	Compd	Time (min)	Yield[b] (%)
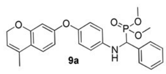 9a	8	95	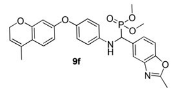 9f	15	95
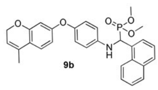 9b	10	94	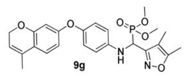 9g	10	95
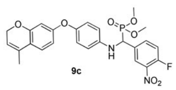 9c	12	93	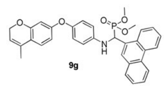 9g	12	95
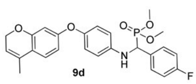 9d	12	95	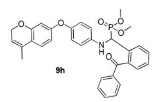 9h	15	94
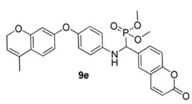 9e	8	93	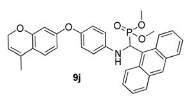 9j	14	96

[a]Reaction between 4-((4-methyl-2*H*-chromen-7-yl)oxy)aniline (**6**) and benzaldehyde (**7a**) and dimethyl phosphite (**8**) without solvent under microwave irradiation.
[*]MW irradiated with 450 W using Catalyst microwave reactor-SSMW1 (Frequency: 2.45 GHz).
[b]Isolated yield.

at 300 W (Entry 4). An 85% yield was obtained with a more noticeable improvement when the power was increased to 350 W (Entry 5). This pattern implied that the increased energy input promoted quicker and more effective molecular interactions, which in turn accelerated the synthesis's condensation and phosphonation processes. Further increasing the microwave power to 400 W (Entry 6) increased the yield to 89%, while 450 W (Entry 7) produced the greatest isolated yield of 95%. Beyond this point, raising the power to 500 W (Entry 8) provided no extra advantage, since the yield remained steady at 95%. This plateau implies that 450 W is the ideal microwave energy for this chemical system, balancing effective energy absorption with the lowest danger of side reactions or breakdown. The observed outcome demonstrates the critical importance of microwave power in driving solvent-free synthesis under regulated conditions. The improved 450 W setting resulted in maximal conversion and selectivity, providing a fast, clean, and high-yielding process for producing the phosphonate derivative **9a**.

The generality of this process to synthesize phosphonates (**9b–j**) in the presence of MW with 4-((4-methyl-2*H*-chromen-7-yl)oxy)aniline (**6**), a variety of aldehydes (**7b**–)

and trimethylphosphite (**8**) in solvent free conditions was investigated after the reaction conditions were optimized and the results were depicted in Table 4.

2.2. General discussion of spectral data for compounds 9a–j

To understand more about the structures of the newly synthesized compounds **9a–j**, NMR (^{1}H, ^{13}C, and ^{31}P), mass, IR spectroscopy, and elemental analyses were used. The ^{31}P NMR spectra of all compounds show a single phosphorus resonance with a δ 22.6–14.6 ppm range, which is consistent with phosphonate esters.[62–64]

The anticipated structural properties were clearly demonstrated by ^{1}H NMR spectroscopy, which was recorded in DMSO-d_6. Because of its location next to the oxygen atom in the pyran ring, the chromene proton H-2 always showed up as a doublet at δ 5.63 ($J = 2.0$ Hz). At δ 5.36 (d, $J = 8.0$ Hz), H-3 was detected, while at δ 5.21 (d, $J = 8.4$ Hz), H-4 resonated. Both showed coupling patterns that validated their vicinal associations. The existence of the amino group on the aryl ring was supported by a clear doublet at δ 5.14 ($J = 8.8$ Hz) that matched the Ar-NH proton. In accordance with P-CH coupling, the methine proton associated with the phosphonate moiety manifested as a well-resolved doublet at δ 4.75 ($J = 10.0$ Hz). Methoxy substituents gave two singlets at δ 3.78 and 3.64, and the chromene methyl group appeared at δ 1.89 as a singlet.

The proton data was supported by[1]3C NMR spectra, which revealed chromene ring carbons at the anticipated chemical shifts. Notably, the electron-rich environment of the oxygenated carbons was reflected by the resonances of C-5 and C-1 at δ 158.13 and δ 155.74, respectively. At δ 67.11 ($J \approx 105$ Hz), the P–CH carbon displayed a distinctive doublet because of its strong interaction with the phosphorus atoms. The presence of methoxy carbons was confirmed by signals at δ 54.15 and δ 52.10, but the chromene methyl carbon was detected at δ 21.52.

Strong and distinctive absorption bands were seen in the IR spectra (KBr): N-H stretching bands, which are suggestive of secondary amine groups, emerged in the 3350–3382 cm^{-1} range. The phosphonate core was supported by the presence of P–O–C stretches close to 1010 cm^{-1} and prominent P = O stretching vibrations between 1210 and 1224 cm^{-1}. The molecular formulae were confirmed by mass spectrometric analysis (LCMS), which produced molecular ion peaks ($M + H^+$) that matched the determined molecular weights of each component. The suggested structures and the high purity of the compounds were further supported by elemental analysis results (C, H, and N) that were within ±0.4% of theoretical values. The identity, purity, and structural integrity of every synthetic chromene-based phosphonate were unquestionably proven by the combined spectroscopic and analytical data (**9a-j**). The Supplementary Materials encompassed standard spectra (^{1}H, ^{31}P, ^{13}C NMR spectra) for compounds **9a**–**j**. (Figures S1–S29).

2.3. Pharmacology

2.3.1. ADME analysis in silico

In Silico ADME analysis uses computational models to predict drug candidates' pharmacokinetic properties, providing numerous advantages in drug discovery. It permits early screening of chemical libraries, which helps in the discovery of interesting compounds while eliminating the need for time-consuming experimental experiments.[65] It also reliably predicts oral bioavailability by evaluating solubility, permeability, and metabolic stability, which is critical for optimizing medication absorption.[66] It also predicts tissue distribution, providing insights into medication spatial distribution and enabling in the formulation of more efficacious molecules.[67] Overall, *in silico* ADME analysis improves decision-making, lowers development costs, and increases clinical trial success rates.

The *in silico* examination of the physicochemical, pharmacokinetic, and drug-likeness features of compounds **9a–j** reveals a highly promising profile for chemical production and biological screening. These compounds were rationally designed with structural features relevant to glycosidase inhibition, as evidenced by their molecular weights (479.5–583.6 g/mol), which, while exceeding the traditional Lipinski threshold, are consistent with other bioactive agents in this class, including the standard reference acarbose (645.6 g/mol). The proposed compounds have a much reduced topological polar surface area (TPSA) (75.83–121.65 Å^2) compared to acarbose (329.01 Å^2), indicating higher passive permeability and oral bioavailability. The presence of sp^3 carbons (Fsp^3: 0.20–0.35) and moderate molar refractivity values (136.05–171.10) indicate a desirable balance between molecular complexity and three-dimensionality, which is generally associated with effective drug-target interaction and pharmacokinetics. Lipophilicity, as evaluated by iLOGP, ranged from 3.85 to 5.57 across the series, demonstrating adequate membrane permeability without surpassing the threshold commonly associated with toxicity or poor solubility. Although several compounds (**9b**, **9e**, **9h**, and **9j**) are projected to be weakly water-soluble or insoluble, such issues can be solved through formulation methods or salt production, especially in early-stage development. (For more information, see Table S1 in the supplementary materials.) All compounds exhibited low anticipated gastrointestinal (GI) absorption, which is a frequent feature of polar or complicated glycomimetic drugs; however, this can be significantly enhanced using prodrug methods or nanoparticle delivery systems. The BOILED-Egg model results provide evaluations for both human stomach absorption and passive blood-brain barrier (BBB) permeability (HIA).[68] Figures S7 and S8 show the boiled egg representation, as well as bio radar images of molecules **9a–j** (see Supplemental materials for details). Notably, all compounds are projected to be non-permeant to the blood-brain barrier (BBB), reducing the possibility of CNS-related side effects, which is a benefit for systemic anti-diabetic therapy.

Assessing the likelihood of substances to behave as substrates or non-substrates for the permeability glycoprotein (PGP), particularly in scenarios requiring migration from the gut wall to the lumen, helps to evaluate active efflux across biological membranes.[69] Several drugs (particularly **9a**–**9g**, **9i**) are projected to be P-gp substrates, which, while potentially restricting oral bioavailability, could aid in minimizing intracellular accumulation and off-target toxicity. In the context of a pharmacokinetic study, it is critical to forecast the possibility for substantial drug interactions caused by the suppression of cytochrome enzymes (CYPs) such as CYP2C19, CYP1A2, CYP2C9, CYP3A4, and CYP2D6, as well as to identify which specific isoenzymes would be affected.[70,71] Some CYP450 interactions were predicted, particularly inhibition of CYP2C9, CYP2D6, and CYP3A4, however such profiles can be managed with careful

Table 5. Drug likeness properties of compounds **9a–j**.

Compounds	Lipinski violations	Ghose violations	Veber violations	Egan violations	Muegge violations	B.S	PAINS alerts	S.A.
9a	0	2	0	1	1	0.55	0	4.93
9b	1	3	0	1	1	0.55	0	5.16
9c	1	3	1	1	1	0.55	0	5.03
9d	0	3	0	1	1	0.55	0	4.91
9e	1	3	0	1	1	0.55	0	5.23
9f	1	3	0	1	1	0.55	0	5.16
9g	0	3	0	1	0	0.55	0	5.25
9h	2	4	0	1	1	0.17	0	5.4
9i	1	4	1	1	1	0.55	0	5.42
9j	2	4	0	1	1	0.17	0	5.4
Acarbose	3	4	2	1	5	0.17	0	7.25

Std*: Acarbose; S.A.: Synthetic Accessibility; B.S.: Bioavailability Score.

optimization and are not unusual among drug candidates in early development. Potts and Guy[72] found a linear relationship between molecule size, Kp, and lipophilicity ($R2 = 0.67$). Among the chemicals in question, **9a**, **9c**, **9d**, **9e**, **9f**, and **9 g** had the highest negative logarithmic Kp values, indicating decreased skin permeability. In contrast, of all the substances tested, the reference medicine had the lowest skin permeability and the highest log Kp value (−16.5). (For more information, see Table S2 in the supplementary materials.)

By evaluating drug-likeness factors, researchers can qualitatively determine whether a compound has the necessary features to become an effective and highly bioavailable oral treatment. As a result, we used a set of five guidelines[73–77] to evaluate the drug-likeness and oral bioavailability of the synthetic compounds. Drug-likeness filters indicated few violations across the Lipinski, Veber, Ghose, Egan, and Muegge criteria. Most compounds had no more than one or two infractions, which is normal for molecules of this size and complexity. Importantly, all compounds cleared the PAINS filter, indicating that they had no known assay-interfering substructures. The bioavailability score (0.55 for the majority of substances) reinforces their drug-like properties, particularly when compared to acarbose (0.17).

The synthetic accessibility (S.A.) values varied from 4.91 to 5.42, indicating that these compounds can be synthesized using typical organic synthesis techniques (Table 5). These *in silico* findings support the design reasoning for compounds **9a–j** and imply a high likelihood of successful synthesis and biological evaluation. Their promising physicochemical features, controlled ADME profiles, and absence of structural liabilities make them ideal candidates for continued development as next-generation glycosidase inhibitors with anti-diabetic potential.

2.3.2. In silico molecular docking study on a-amylase enzyme

We tested all produced compounds *in silico* against the pancreatic α-amylase enzyme using the 1-click docking web server application,[78] which is well-known for being compatible with the AutoDock Vina docking technique. Significant improvements in binding energies compared to the reference drug, acarbose (−8.2 kcal/mol), were found in the screening data. In particular, every chemical had binding energies between −9.3 and −8.0 kcal/mol that were either superior or almost equal. Table S3 in the supplemental materials provides detailed information about these binding energies and the constant complex bonding postures.

Among the compounds under investigation, compounds **9b**, **9c**, **9e**, **9f**, **9 g**, **9h**, and **9j** have demonstrated the best binding interactions, suggesting a strong potential for enzyme inhibition. The binding energies of the chemicals in the title are organized as follows: **9 g** (8.5 kcal/mol) = **9h** (8.5 kcal/mol) > **9i** (8.2 kcal/mol) > **9a** (8.0 kcal/mol) > **9d** (8.0 kcal/mol) = **9j** (−9.3 kcal/mol) > **9e** (−9.0 kcal/mol) > **9b** (−8.9 kcal/mol) > **9c** (−8.9 kcal/mol) > **9f** (8.5 kcal/mol) = **9 g** and 8.5 kcal/mol). We looked at particular ligand–protein interactions, such as π–π stacking, hydrogen bonding, hydrophobic contacts, and electrostatic interactions, to better understand the binding mechanism.

By creating a hydrogen bond with GLN63, 9b showed the strongest binding affinity of all the chemicals examined, which could help the ligand-enzyme complex become more stable and specific. Furthermore, **9b** demonstrated π-π stacking interaction with TRP59, an aromatic residue that is known to be essential for stabilizing inhibitors in the α-amylase active site. Effective occupation of the hydrophobic pocket of the enzyme was demonstrated by this compound's substantial hydrophobic contacts with important residues, including LEU165, LEU162, ALA198, VAL234, ILE235, TYR151, TRP59, TRP58, and TYR62. Despite the absence of hydrogen bonding, **9f** was compensated by significant hydrophobic interactions with ALA307, LEU237, ILE235, TYR151, and ALA198, as well as strong π-π stacking with TRP59. TRP59, TRP58, LEU162, LEU165, and TYR62, which collectively probably provide a substantial contribution to its binding strength. With HIS201, a residue close to the catalytic site, **9j** displayed π-π stacking, which would increase its capacity to obstruct enzymatic activity. 9j's significant binding potential was further supported by interactions with LEU165, LEU162, VAL234, ILE235, ALA198, TYR151, TRP59, and TRP58 that were part of its hydrophobic network. Likewise, **9e** demonstrated hydrophobic interactions with ALA307, VAL234, ILE235, ALA198, TYR151, LEU165, LEU162, TRP59, and TRP58, as well as π-π stacking with TRP59, indicating an excellent match inside the active site. The formation of a hydrogen bond between **9h** and TYR151, as well as hydrophobic interactions with ILE235, TYR151, LEU162, TRP58, TRP59, and TYR62, significantly increased binding specificity. Docking research shows that molecules having π-π stacking and hydrophobic contacts, especially with important residues like TRP59, LEU165, ALA198, and TYR151, are more efficient at inhibiting α-amylase activity. These chemicals' interaction characteristics suggest they could be effective α-amylase inhibitors. These interactions are summarized in Table 6.

Table 6. Molecular docking interactions of synthesized compounds with α-amylase.

Compounds	Hydrogen bonding	π–π stacking	Hydrophobic interactions
9b	GLN63	TRP59	LEU165, LEU162, ALA198, VAL234, ILE235, TYR151, TRP59, TRP58, TYR62
9c	NONE	NONE	LEU165, LEU162, ALA198, VAL234, ILE235, TYR151, TYR151, TRP59, TRP58, TYR62
9e	NONE	TRP59	ALA307, VAL234, ILE235, ALA198, TYR151, LEU165, LEU162, TRP59, TRP58
9f	NONE	TRP59	ALA307, LEU237, ILE235, TYR151, ALA198, LEU162, LEU165, TRP59, TRP58, TYR62
9g	NONE	NONE	LEU165, LEU162, ALA307, VAL234, ILE235, ALA198, TYR151, TRP59, TRP58
9h	TYR151	NONE	ILE235, TYR151, LEU162, TRP58, TRP59, TYR62
9j	NONE	HIS201	LEU165, LEU162, VAL234, ILE235, ALA198, TYR151, TRP59, TRP58

These findings give insight on how synthetic compounds block pancreatic α-amylase through intricate chemical interactions. This provides valuable insights into future drug design and optimization. 2D ligand diagrams provide visual representations of these binding contacts, which helps to explain the observed interactions (See Table S4 in supplemental materials for details).

2.3.3. In silico molecular docking study on α-glucosidase enzyme

Using the 1-Click Docking web server (http://mcule.com/apps/1-click-docking/), *in silico* molecular docking was used to assess the binding capability of the produced compounds with the pancreatic α-glucosidase enzyme. The AutoDock Vina docking technique was used to confirm the results.[78] All of the compounds **9a–j** had binding energies between −10.1 and −8.5 kcal/mol, according to the docking data, which was better than that of the reference drug, acarbose. For comprehensive details on molecular interactions and binding energies, see Table S4 (see supplemental materials).

The binding energy of the title compounds is in the order of **9e** (−10.1 kcal/mol) > **9h** (**−**9.9 kcal/mol**)** > **9i** (−9.8 kcal/mol) > **9b** (−9.8 kcal/mol) > **9j** (9.7 kcal/mol**)** > **9d (−**9.7 kcal/mol) > **9f** (−9.6 kcal/mol) > **9c** (−8.9 kcal/mol) > **9a** (−8.7 kcal/mol) > **9 g** (−8.5 kcal/mol). We studied specific ligand-protein interactions, including π–π stacking, hydrogen bonding, hydrophobic contacts, and π-Cation interactions, to better understand the binding mechanism. These interactions are summarized in Table 7. The molecular docking investigation of produced α-aminophosphonates against α-glucosidase revealed varied interaction patterns, potentially contributing to their inhibitory actions. Compound **9b** formed a hydrogen bond with LYS A:352 and had a π-cation interaction with HID A:342, as well as hydrophobic interactions with ALA A:349, PHE A:516, ALA A:444, ALA A:514, PRO A:442, ALA A:434, LEU A:433, and ALA B:451, indicating substantial stabilization inside the enzyme's active site. **9d** exhibited hydrogen bonding with ASP A:441, a π-cation contact with LYS

Table 7. Molecular docking interactions of synthesized compounds with α-glucosidase.

Compounds	Hydrogen bonding	π–π Stacking	π-Cation interaction	Hydrophobic interactions
9b	LYS A:352	None	HID A:342	ALA A:349, PHE A:516, ALA A:444, ALA A:514, PRO A:442, ALA A:434, LEU A:433, ALA B:451
9d	ASP A:441	None	LYS A:352	ALA B:454, PHE A:516, ALA A:444, ALA A:514, PRO A:442, ALA A:434, LEU A:433, ALA B:451
9e	ASN B:441	None	LYS A:352	ALA A:454, PHE A:516, PHE A:516, ALA A:349, ALA B:454, ALA B:451, PRO B:442, PRO A:442
9f	ASN B:447	None	None	ALA A:349, PHE A:516, ALA A:514, ALA A:444, PRO A:442, ALA B:454, ALA B:451, PRO B:442
9h	None	HID A:348	None	PHE A:516, ALA A:514, TYR A:530, ALA A:529, ALA B:514, ALA B:454, ALA B:451
9i	None	PHE A:516	LYS A:352	LEU A:433, PHE B:455, ALA B:454, PHE A:516, ALA A:444, ALA A:514, ALA B:451, ALA A:349
9j	None	None	LYS A:352	LEU A:373, LEU A:433, PHE B:455, ALA B:454, PHE A:516, ALA A:514, ALA B:514, ALA B:451, ALA A:349

A:352, and hydrophobic interactions with residues including ALA B:454, PHE A:516, ALA A:444, ALA A:514, PRO A:442, ALA A:434, LEU A:433, and ALA B:451, indicating strong engagement with the catalytic pocket. **9e** had a hydrogen bond with ASN B:441, a π-cation interaction with LYS A:352, and strong hydrophobic contacts with ALA A:454, PHE A:516 (dual interactions), ALA A:349, ALA B:454, ALA B:451, PRO B:442, and PRO A:442, indicating adequate active site accommodation. Despite missing hydrogen bonding and π-cation interaction, **9f** showed strong hydrophobic contacts with ALA A:349, PHE A:516, ALA A:514, ALA A:444, PRO A:442, ALA B:454, ALA B:451, and PRO B:442, showing binding driven mostly by hydrophobic forces. **9h** formed π-π stacking with HID A:348 and hydrophobically interacted with PHE A:516, ALA A:514, TYR A:530, ALA A:529, ALA B:514, ALA B:454, and ALA B:451, emphasizing the relevance of aromatic and hydrophobic interactions in complex stabilization. **9i** shows π-π stacking with PHE A:516, a π-cation interaction with LYS A:352, and hydrophobic interactions with LEU A:433, PHE B:455, ALA B:454, PHE A:516, ALA A:444, ALA A:514, ALA B:451, and ALA A:349, indicating its potential as an α-glucosidase inhibitor. **9j** had a π-cation contact with LYS A:352 and extensive hydrophobic interactions with LEU A:373, LEU A:433, PHE B:455, ALA B:454, PHE A:516, ALA A:514, ALA B:514, ALA B:451, and ALA A:349, indicating efficient binding within the enzyme's hydrophobic pocket.

These findings suggest that hydrophobic interactions, particularly with PHE A:516, ALA A:514, ALA B:451, and ALA B:454, as well as π-cation and infrequent π-π stacking interactions, play a significant role in the inhibitory capacity of these compounds.

In systematic literature, 2D diagrams are used to determine the target protein's binding interactions with ligands. Table S6 of supplemental materials displays the 2D ligand diagrams for molecules **9b**, **9d**, **9e**, **9f**, **9h**, **9i**, and **9j** are indicating their interactions with the target enzyme.

2.3.4. α-Amylase inhibitory activity study of compounds 9a–j and structure–activity relationship (SAR) analysis

The synthesized compounds were examined *in vitro* for their ability to inhibit α-amylase using a modified version of a typical procedure.[79,80] They were evaluated for their α-amylase inhibitory potential in comparison with the standard drug, acarbose ($IC_{50} = 103.29$ μg/mL). The IC_{50} values of the tested compounds ranged from 99.24 to 142.54 μg/mL, indicating varying levels of inhibition. Among the series, compound **9e** exhibited the most potent inhibitory activity with an IC_{50} value of 99.24 μg/mL, outperforming acarbose. Close behind were **9j** ($IC_{50} = 101.07$ μg/mL) and **9c** ($IC_{50} = 101.84$ μg/mL), which also demonstrated strong inhibition. **9j** and **9c**, with $IC_{50} = 101.07$ and 101.84 μg/mL, respectively, showed significant inhibition. Compound **9i**, with a large N-heterocyclic substituent, had the lowest activity ($IC_{50} = 142.54$ μg/mL), indicating steric hindrance or low binding affinity at the enzyme active site (Figure 2).

The structure–activity relationship (SAR) investigation found numerous significant behaviors. Compounds containing electron-rich or planar aromatic rings, such as **9e** (3-furyl) and **9j** (naphthyl), shown improved inhibitory potential, possibly due to advantageous π–π stacking or hydrophobic interactions with the α-amylase active site. The presence of electron-drawing groups (e.g. –F and $–NO_2$ in **9c**) contributed

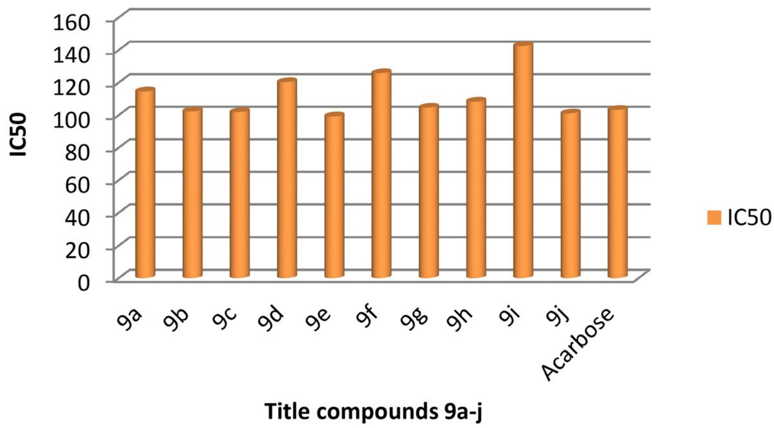

Figure 2. IC_{50} values of compounds **9a**–**j**.

favorably, probably by increasing binding affinity through dipole interactions. Compounds having sterically demanding or non-aromatic substituents, such as **9i** with a bulky N-containing ring system, shown lower activity, implying that excessive bulk interferes with enzyme interaction. The moderate performance of phenyl derivatives such as **9a** ($IC_{50} = 114.55$ μg/mL) and **9d** ($IC_{50} = 120.28$ μg/mL) demonstrates that basic aromatic moieties provide baseline activity but require further substitution for improved potency. In summary, chromone-based phosphoramidates' α-amylase inhibitory activity is heavily impacted by the substituents on the aryl/heteroaryl group, including their type, size, and electronic characteristics. These findings help to develop more efficient enzyme inhibitors by selecting planar, conjugated, and moderately electron-withdrawing aromatic groups at the phosphonate moiety.

2.3.5. Statistical analysis of α-amylase inhibition assay

α-Amylase inhibitory activity of **9a–j** was examined statistically using one-way ANOVA and Tukey's HSD post hoc test to determine the significance of differences in IC_{50} values. The ANOVA results showed a substantial variance in the mean IC_{50} values across the investigated drugs ($F = 23{,}693.80$, $p < 0.0001$), showing that structural alterations affect inhibitory potency. Tukey's HSD test revealed that compound **9e** had the highest activity ($IC_{50} = 99.24$ μg/mL), significantly outperforming other derivatives and the standard medication Acarbose ($IC_{50} \approx 103.29$ μg/mL). Compound **9j** displayed considerable action, similar to **9e**, while compounds **9i** and **9f** had weaker inhibition with significantly larger IC_{50} values. These statistical findings confirm the biochemical assay results and support the structure–activity relationship (SAR) analysis, emphasizing the essential function of particular substituents in modifying α-amylase inhibitory activity (Figure 3).

2.3.6. In vitro α-glucosidase inhibitory activity study of compounds 9a–j and structure–activity relationship (SAR) analysis

Using acarbose as the reference standard, the synthesized compounds **9a–j** were tested for their α-glucosidase inhibitory potential[81] at concentrations ranging from 25 to 250 μg/mL. Their inhibitory efficacy was measured using the IC_{50} values. With an IC_{50} value of 88.89 μg/mL, which is less than that of acarbose (93.27 μg/mL), compound **9e**

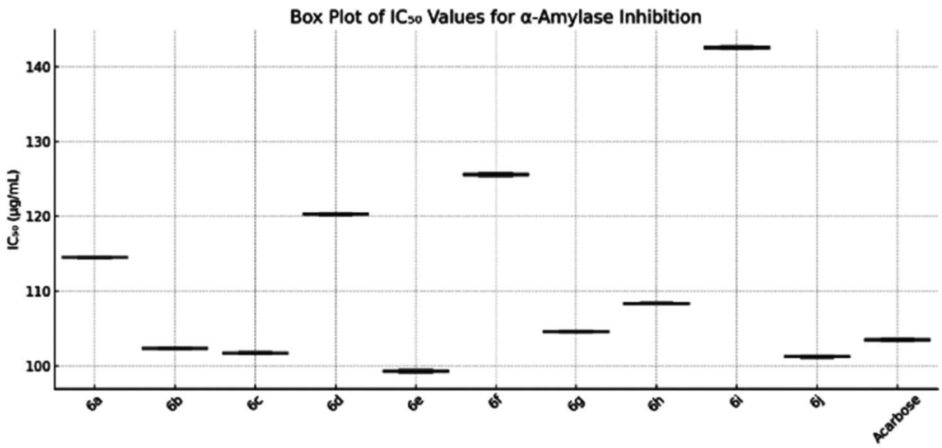

Figure 3. Box plot of IC_{50} values for *α*-amylase inhibition.

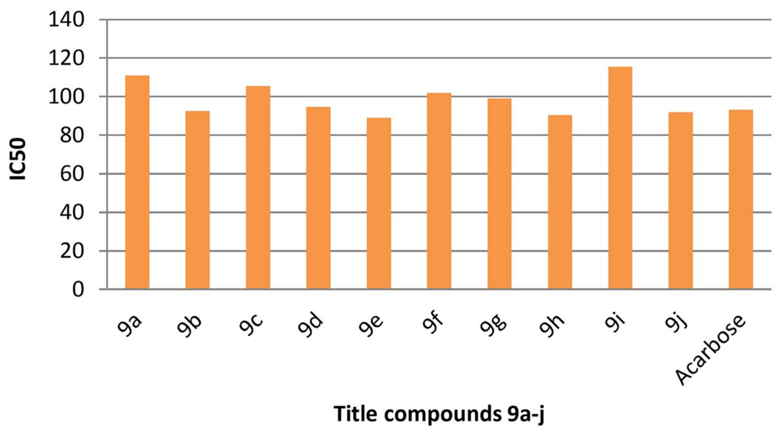

Figure 4. IC_{50} values of compounds **9a**–**j**.

was shown to be the most effective inhibitor among the compounds examined. Other compounds that showed IC_{50} values that were on par with or marginally better than the standard medication were **9h** (90.45 µg/mL), **9b** (92.6 µg/mL), **9j** (91.77 µg/mL), and **9d** (94.54 µg/mL). Conversely, the inhibitory effects of compounds **9a** (111.02 µg/mL), **9c** (105.49 µg/mL), and **9i** (115.52 µg/mL) were comparatively weaker (Figure 4). According to these findings, some of the compound series' members appear to have promising α-glucosidase inhibitory action and may be used as lead structures for more optimization.

A thorough structure–activity relationship (SAR) analysis of compounds **9a-j** shows that the position of aldehyde moiety and type of substituent has a crucial impact on the inhibitory activity of α-glucosidase. Superior inhibition was shown by compounds containing heteroaromatic rings, such as **9e** (furan) and **9h** (pyridyl), most likely as a result of improved hydrogen bonding or π–π stacking interactions with the enzyme's active site. Strong activity was also demonstrated by compound **9b**, which has a naphthyl ring. This could be explained by the prolonged π-conjugation increasing binding affinity. However, the comparatively low activity of **9a** (phenyl) and **9c** (fluoro-nitro substituted phenyl) suggests that strong electron-withdrawing groups or simple aromatic systems could not promote the best binding. Furthermore, **9i**, which has a large biphenyl moiety, exhibited the least amount of activity, indicating that steric hindrance may hinder efficient enzyme interaction. Overall, the SAR indicates that α-glucosidase inhibitory potency can be greatly increased by adding heteroatoms and enhancing steric and electronic variables in the aryl aldehyde section.

2.3.7. Statistical analysis of α-glucosidase inhibition assay

The inhibitory activity of compounds **9a–j** against α-glucosidase was measured in triplicate and expressed as IC_{50} values (μg/mL). Across the chemical series, the mean IC_{50} values varied, suggesting varying levels of enzyme inhibition. The mean IC_{50} values of the synthesized compounds and the reference medication, acarbose, were compared using a one-way Analysis of Variance (ANOVA) to see if there were any statistically significant differences. At least one chemical had a significantly distinct inhibitory profile, according to the ANOVA test, which showed a significant difference ($p < 0.05$). Tukey's Honestly Significant Difference (HSD) post hoc test was used to pinpoint certain group differences. The findings showed that compound **9e** ($IC_{50} = 88.83$ μg/mL) greatly outperformed the majority of other compounds, including the common Acarbose ($IC_{50} = 93.29$ μg/mL), in terms of α-glucosidase inhibition. In contrast to both **9e** and Acarbose, compound **9i** showed the poorest inhibition ($IC_{50} = 115.64$ μg/mL), indicating decreased effectiveness. The IC_{50} distribution for each drug is shown graphically in the box plot below. It amply demonstrates compound **9e**'s tighter range and lower median, substantiating its superior activity profile. These findings lend support to compound **9e**'s potential as a promising lead for more α-glucosidase inhibitor research. The discovered differences indicate a strong structure–activity relationship that warrants further exploration (Figure 5).

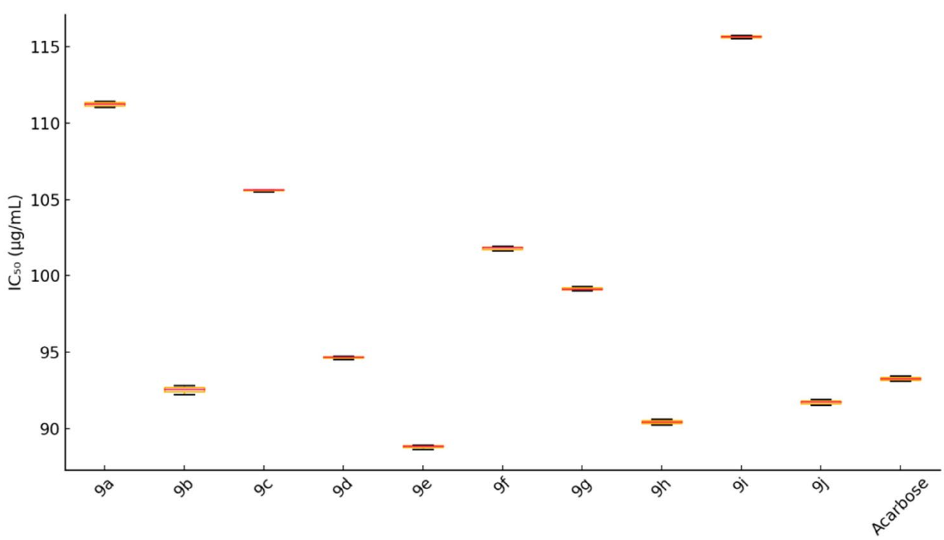

Figure 5. Box plot of IC_{50} values for α-glucosidase inhibition.

3. Experimental

3.1. Instrumentation and materials

All reagents and solvents, unless specified, were purchased from Sd. Fine Chem. Ltd. and Sigma Aldrich, India, and used without further purification. The nano ZnO (particle size <100 nm) used was supplied by Sigma Aldrich. All reactions were conducted using a magnetic stirrer with a heated plate, and the purity of the finished product was assessed using TLC on silica gel Al sheets. Microwave-assisted reactions were carried out in a Catalyst Microwave Reactor (SSMW1 type). A Bruker AMX spectrometer was used to record NMR spectra (^{1}H at 400 MHz, ^{13}C at 100 MHz, and ^{31}P at 161.9 MHz) with DMSO-d_6 as the solvent and TMS as the internal standard. Using KBr pellets, IR spectra were obtained on a Bruker IFS 55 (Equinox) FT-IR spectrophotometer, elemental analyses were performed on a Thermo Fisher Flash 1112 CHN analyzer, and LC–MS spectra were captured on a Shimadzu LCMS-2010A system. The Supplementary Information contains all of the analytical data, instrumentation specifications, and experimental details.

3.2. Procedures

3.2.1. Synthesis of 4-methyl-2H-chromen-7-ol

1.10 g (10 mmol) of resorcinol was added to a 50 mL round-bottom flask (**1**). To create a uniform solution, the mixture was vigorously stirred after adding ethyl acetoacetate (**2**) (1.30 g, 1.15 mL, 10 mmol). Two to three drops of concentrated sulfuric acid, or around 0.1 mL, were added as a catalyst. The reaction mixture was heated for three hours, stirring occasionally, in an oil bath maintained between 100 °C and 120 °C. The evolution of the reaction could be tracked using thin-layer chromatography (TLC) on silica gel plates with hexane:ethyl acetate (3:1) as the mobile phase. Once the reaction mass was complete, it was allowed to cool to ambient temperature and then slowly added to 50 milliliters of ice-cold water while being aggressively agitated. Filtration was used to collect the resulting pale yellow solid, which was then thoroughly cleaned with cold water and vacuum-dried. The refined 4-methyl-7-hydroxycoumarin (**3**) was obtained by recrystallizing the crude product from 20 mL of heated ethanol. M.P.190-192 °C.

Anhydrous tetrahydrofuran (THF, 15 mL) was used to suspend lithium aluminum hydride ($LiAlH_4$, 0.50 g, 13 mmol) in a dry 100 mL three-neck round-bottom flask equipped with a nitrogen inlet and reflux condenser. In an ice bath, the suspension was cooled to 0 °C. Dropwise additions of a 4-methyl-7-hydroxycoumarin (**3**) solution (1.74 g, 10 mmol) in THF (15 mL) were made over a period of 15–20 min while maintaining an internal temperature below 5 °C. After the addition, the mixture was stirred for three hours at room temperature while TLC (silica gel, hexane:ethyl acetate 3:1) tracked the reaction. To further break down the excess hydride, two milliliters of water were added dropwise, followed by ten more milliliters of water. After the mixture was extracted using 20 mL of ethyl acetate, the organic layer was separated, washed with 10 mL of brine, and dried over anhydrous sodium sulfate. After the solvent was extracted at low pressure, 4-methyl-2*H*-chromen-7-ol (**4**) was produced as a pure product using column chromatography on silica gel with hexane:ethyl acetate (7:3) as the eluent. Solid, M.P. 170-173 °C

3.2.2. Synthesis of 4-((4-methyl-2H-chromen-7-yl)oxy)aniline (6)

A solution of 4-methyl-2*H*-chromen-7-ol (**4**) (1.62 g, 10 mmol) in anhydrous tetrahydrofuran (THF, 15 mL) was prepared in a 50 mL round-bottom flask. Over the course of 15 minutes, 4-chloroaniline (**5**) (1.27 mL, 10 mmol) was added dropwise to THF (10 mL) while being continuously stirred. The reaction's base was tetramethylguanidine (TMG, 10 mmol, 1.14 g), and the temperature was maintained between 5 and 10 °C using an ice bath. The reaction mixture was stirred for three more hours at the same temperature after the addition was finished. TLC was used to monitor the reaction's progress until it was complete (silica gel; hexane:ethyl acetate, 2:3). Pure 4-((4-methyl-2*H*-chromen-7-yl)oxy)aniline (**6**) was obtained by recrystallizing the crude product from 20 milliliters of hot ethanol after the precipitated tetramethylguanidine hydrochloride was filtered out of the resulting mixture. Solid; yield, 90%; melting point: 158–160 °C.

δ_H (DMSO-d_6): 7.24 (d, 1H, chromene-H), 6.83 (d, J = 7.2 Hz, 2H, Ar-H), 6.71 (d, J = 7.6 Hz, 2H, Ar-H), 6.67 (s, 1H, Ar-H), 6.60 (d, 1H, Ar-H), 6.23 (s, 2H, Ar-NH_2), 5.62 (d, J = 2.0 Hz, 1H, chromene-H), 5.34 (d, J = 8.0 Hz, 1H, chromene-H), 5.20 (d, J = 8.4 Hz, 1H, chromene-H), 1.85 (s, 3H, chromene-CH_3); δ_C (DMSO-d_6): 155.63 (C-1), 108.51 (C-2), 124.25 (C-3), 105.42 (C-4), 154.43 (C-5), 126.86 (C-6), 72.46 (C-8), 117.93 (C-9), 128.25 (C-10), 21.34 (C-11), 145.24 (C-13), 114.52 (C-14), 120.71 (C-15), 140.80 (C-16), 122.34 (C-17), 115.91 (C-18).

3.2.3. Synthesis of phosphonates (9a–j) using microwave irradiation method

Tetrahydrofuran (THF, 10 mL) was combined with 4-(4-Methyl-2*H*-chromen-7-yl)oxy) aniline (**6**) (2.17 g, 10 mmol) and benzaldehyde (**7a**) (1.06 mL, 10 mmol) in a 100 mL round-bottom flask. This solution was agitated while dimethyl phosphite (**8**) (1.28 mL, 10 mmol) was added dropwise. The reaction mixture was subjected to 450 W of microwave radiation for 10 minutes at room temperature without the use of solvents in a Catalyst microwave reactor (SSMW1). The progress of the reaction was monitored by TLC (hexane:ethyl acetate, 3:2). After finishing, the reaction mixture was washed with 15 mL of water and allowed to cool to room temperature. The organic layer was separated, dried over anhydrous sodium sulfate, and then concentrated at 50 °C with a lower pressure. Pure dimethyl (((4-((4-methyl-2*H*-chromen-7-yl)oxy)phenyl)amino)(phenyl)methyl)phosphonate (**9a**) as a solid was obtained by purifying the crude residue by column chromatography on silica gel with hexane:ethyl acetate (7:3) as the eluent (Figure 6).

*3.3. Characterization of title compound 9a–j. Dimethyl (((4-((4-methyl-2H-chromen-7-yl)oxy)phenyl)amino)(phenyl)methyl)phosphonate (**9a**):* solid. M.P. 151–157 °C. Yield: 97%. δ_H (DMSO-d_6): 7.43 (d, J = 7.2 Hz, 2H, Ar-H), 7.33 (d, J = 7.2 Hz, 1H, Ar-H), 7.28 (d, J = 7.2 Hz, 2H, Ar-H), 7.26 (d, J = 7.6 Hz, 1H, Ar-H), 6.93 (d, J = 7.6 Hz, 2H, Ar-H), 6.79 (d, J = 7.6 Hz, 2H, Ar-H), 6.75 (d, J = 7.2 Hz, 1H, Ar-H), 6.64 (s, J = 6.8 Hz, 1H, Ar-H),

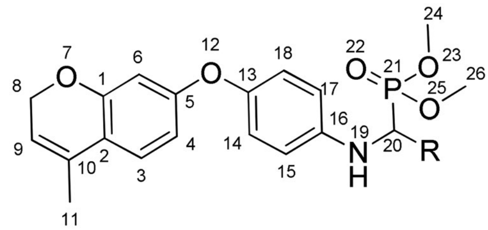

Figure 6. General structure of compound **9a–j**.

5.63 (d, $J = 2.0$ Hz, 1H, chromene-H), 5.36 (d, $J = 8.0$ Hz, 1H, chromene-H), 5.21 (d, $J = 8.4$ Hz, 1H, chromene-H), 5.14 (d, $J = 8.8$ Hz, 1H, Ar-NH), 4.75 (d, $J = 10.0$ Hz, 1H, methine-H), 3.78 (s, 3H, $-OCH_3$), 3.64 (s, 3H, $-OCH_3$), 1.89 (s, 3H, chromene-CH_3); δ_C (DMSO-d_6): 158.13 (C-5), 155.74 (C-1), 145.37 (C-13), 139.35 (C-16), 135.54 (C-27), 129.34 (C-29 & C-31), 128.42 (C-10), 127.39 (C-3), 127.26 (C-28 & C-32), 126.45 (C-6), 125.78 (C-30), 118.45 (C-9), 116.54 (C-18), 114.87 (C-14), 113.75 (C-17), 113.46 (C-15), 110.78 (C-4), 107.23 (C-2), 73.17 (C-8), 67.11 ((d, $J = 105.3$ Hz, C-20), 54.15 (C24), 52.10 (C-26), 21.52 (C-11). δ_P (DMSO-d_6): 14.64 ppm; IR (KBr) (ν_{max} cm^{-1}): 3350 (NH), 1245 (C–O), 1211 (P=O), 1012 (P–O–C_{alip}); LCMS (*m/z*, %): 452.45 ($(M + H)^+$, 100); Anal. Calcd. for $C_{25}H_{26}NO_5P$; calcd: C, 66.51; H, 5.80; N, 3.10%; found: C, 66.62; H, 5.70; N, 3.21%.

3.4. In silico ADME analysis

The Swiss ADME tool, created by the Swiss Institute of Bioinformatics (http://www.sib.swiss), was used to computationally predict the physicochemical properties, lipophilicity, water solubility, pharmacokinetics/ADME, drug-likeness, and medicinal chemistry features of all the suggested compounds.

3.5. In silico molecular docking studies

In silico molecular docking was used to investigate **9a–j**'s binding mechanism with pancreatic α-amylase (PDB ID: 3IJ8) and α-glucosidase (PDB ID: 3WY1). The enzymes' crystal structures were retrieved from the RCSB Protein Data Bank (PDB ID: 3IJ8 and PDB ID: 3WY1). To increase efficiency, water molecules, heteroatoms, and cofactors were removed from the structure. Charges, hydrogen bonds, and missing atoms were included. The 1-Click docking web server tool (https://mcule.com) was used with the default binding site centers X: 7.2178, Y: 16.2957, and Z: 42.1167 and X: 3.391, Y: 1.31, and Z: −8.362 respectively for docking investigations on α-amylase and α-glucosidase enzymes. The discovery studio visualizer V16.1.0.15350 was used to explore the process of docking ligands with proteins and their interactions.

3.6. α-Amylase and α-glucosidase inhibitory activity

The novel compounds' inhibitory efficacy against α-amylase and α-glucosidase was investigated using known methods with minimal modifications. (For a detailed process, go to Supplemental Materials.) The half-maximal inhibitory concentration (IC_{50}) is a very good measure of a drug's potency. It is a measure of antagonist drug potency in pharmacological research since it indicates how much drug is necessary to inhibit a biological function by half. The IC_{50} values in this study were calculated by plotting concentration (*X*-axis) against percent inhibitory activity (*Y*-axis). The IC_{50} value is calculated by applying the linear ($y = mx + c$) equation to this graph at $y = 50$. A one-way ANOVA test was used to determine the overall significance of differences across compounds, followed by Tukey's HSD post hoc test for pairwise comparisons.

4. Conclusion

We developed an environmentally friendly and effective synthesis technique to produce a new family of α-aminophosphonates (**9a–j**). This methodology takes a solvent-free, catalyst-minimized approach, with microwave irradiation greatly accelerating the reaction process and increasing product yield. The transformation follows the Kabachnik–Fields (K-F) reaction pathway, providing an environmentally friendly option that adheres to green chemistry principles by removing the use of toxic organic solvents and lowering waste generation. To assess the drug-likeness of the synthesized compounds, *in silico* molecular docking studies were used in conjunction with ADMET (Absorption, Distribution, Metabolism, Excretion, and Toxicity) predictions. These computer studies identified numerous substances with acceptable pharmacokinetic characteristics and probable safety, indicating their suitability for further research. Enzymatic inhibition experiments were used to investigate the biological potential of produced α-aminophosphonates, which target two carbohydrate-degrading enzymes linked to type 2 diabetes: α-glucosidase and α-amylase. The in vitro results showed that many of these compounds had significant inhibitory action against both enzymes. Among the series, compound **9e** exhibited the most potent inhibitory activity against α-amylase with an IC_{50} value of 99.24 μg/mL, outperforming acarbose. Close behind were **9j** ($IC_{50} = 101.07$ μg/mL) and **9c** ($IC_{50} = 101.84$ μg/mL), which also demonstrated strong inhibition. In α-glucosidase inhibitory activity, with an IC_{50} value of 88.89 μg/mL, which is less than that of acarbose (93.27 μg/mL), compound **9e** was shown to be the most effective inhibitor among the compounds examined. Other compounds that showed IC_{50} values that were on par with or marginally better than the standard medication were **9h** (90.45 μg/mL), **9b** (92.6 μg/mL), **9j** (91.77 μg/mL), and **9d** (94.54 μg/mL). Interestingly, certain molecules outperformed the reference anti-diabetic medication, acarbose. Compound **9e** inhibited α-glucosidase the most, with an IC_{50} value of 88.89 μg/mL. Compound **9j** also inhibited α-glucosidase and α-amylase, indicating its potential as a broad-spectrum anti-diabetic drug.

A comprehensive structure–activity relationship (SAR) analysis revealed that the addition of heteroaromatic rings and electron-donating substituents to the aryl aldehyde moiety considerably increased enzyme inhibitory activity. In contrast, the inclusion of bulky groups or highly electron-withdrawing substituents was observed to reduce biological efficacy. These findings highlight the need of making sensible structural changes at the aryl aldehyde position to improve anti-diabetic action. This study offers useful insights into designing multifunctional α-aminophosphonate scaffolds as potential options for developing next-generation anti-diabetic therapies.

Acknowledgements

The authors thank Dr. S. Someswar Rao, Department of Genetics of Osmania University for his assistance with bioactivity investigations and Dr. C. Naga Raju, Department of Chemistry, S. V. University for his unwavering support throughout the completion of this work.

Author contributions

CRediT: **Manjula Kavala:** Investigation, Methodology, Validation, Visualization, Writing – original draft; **Raja Rajeswari Tiruveedula:** Investigation, Methodology, Project administration, Supervision, Writing – review & editing; **Chennamsetty Subramanyam:** Data curation, Investigation, Software, Writing – review & editing.

Disclosure statement

No potential conflict of interest was reported by the authors.

ORCID

Raja Rajeswari T. http://orcid.org/0000-0001-7569-9758

References

[1] Chatterjee, S.; Khunti, K.; Davies, M. J. Type 2 Diabetes. *Lancet* **2017**, *389*, 2239–2251. DOI: 10.1016/S0140-6736(17)30058-2.
[2] Duarte, A. M.; Guarino, M. P.; Barroso, S.; Gil, M. M. Phytopharmacological Strategies in the Management of Type 2 Diabetes. *Foods* **2020**, *9*, 271. DOI: 10.3390/foods9030271.
[3] Chikara, G.; Sharma, P. K.; Dwivedi, P.; Charan, J.; Ambwani, S.; Singh, S. A Narrative Review of Potential Future Antidiabetic Drugs: should we Expect More? *Indian J. Clin. Biochem.* **2018**, *33*, 121–131. DOI: 10.1007/s12291-017-0668-z.
[4] Saeedi, M.; Hadjiakhondi, A.; Nabavi, S. M.; Manayi, A. Heterocyclic Compounds: effective α-Amylase and α-Glucosidase Inhibitors. *Curr. Top. Med. Chem.* **2017**, *17*, 428–440. DOI: 10.2174/1568026616666160824104655.
[5] Chaudhury, A.; Duvoor, C.; Dendi, V. S. R.; Kraleti, S.; Chada, A.; Ravilla, R.; Marco, A.; Shekhawat, N. S.; Montales, M. T.; Kuriakose, K.; et al. Clinical Review of Antidiabetic Drugs: implications for Type 2 Diabetes Mellitus Management. *Front. Endocrinol.* **2017**, *8*, 12. DOI: 10.3389/fendo.2017.00006.
[6] Santos, C. M. M.; Proença, C.; Freitas, M.; Araújo, A. N.; Silva, A. M. S.; Fernandes, E. Inhibition of the Carbohydrate-Hydrolyzing Enzymes α-Amylase and α-Glucosidase by Hydroxylated Xanthones. *Food Funct.* **2022**, *13*, 7930–7941. DOI: 10.1039/d2fo00023g.
[7] Dhameja, M.; Gupta, P. Synthetic Heterocyclic Candidates as Promising α-Glucosidase Inhibitors: An Overview. *Eur. J. Med. Chem.* **2019**, *176*, 343–377. DOI: 10.1016/j.ejmech.2019.04.025.
[8] Santos, C. M. M.; Freitas, M.; Fernandes, E. A Comprehensive Review on Xanthone Derivatives as α-Glucosidase Inhibitors. *Eur. J. Med. Chem.* **2018**, *157*, 1460–1479. DOI: 10.1016/j.ejmech.2018.07.073.
[9] Ghani, U. Re-Exploring Promising α-Glucosidase Inhibitors for Potential Development into Oral anti-Diabetic Drugs: finding Needle in the Haystack. *Eur. J. Med. Chem.* **2015**, *103*, 133–162. DOI: 10.1016/j.ejmech.2015.08.043.
[10] Drugbank. https://go.drugbank.com (accessed Sept 20, 2023).
[11] Kokil, G. R.; Rewatkar, P. V.; Verma, A.; Thareja, S.; Naik, S. R. Pharmacology and Chemistry of Diabetes Mellitus and Antidiabetic Drugs: A Critical Review. *Curr. Med. Chem.* **2010**, *17*, 4405–4423. DOI: 10.2174/092986710793361225.

[12] Hossain, M. A.; Pervin, R. Current antidiabetic drugs: Review of their efficacy and safety. In nutritional and therapeutic interventions for diabetes and metabolic syndrome, 2nd ed.; Bagchi, D.; Nair, S., Eds.; Academic Press: Cambridge, MA, USA, 2018; Chapter 34, pp. 455–473.
[13] Asano, N. Sugar-Mimicking Glycosides Inhibitors: bioactivity and Application: A Review. *Cell. Mol. Life Sci.* **2009**, *66*, 1479–1492. DOI: 10.1007/s00018-008-8522-3.
[14] Proença, C.; Ribeiro, D.; Freitas, M.; Fernandes, E. Flavonoids as Potential Agents in the Management of Type 2 Diabetes through the Modulation of α-Amylase and α-Glucosidase Activity, a Review. *Crit. Rev. Food Sci. Nutr.* **2022**, *62*, 3137–3207. DOI: 10.1080/10408398.2020.1862755.
[15] Dirir, A. M.; Daou, M.; Yousef, A. F.; Yousef, L. F. A Review of Alphaglucosidase Inhibitors from Plants as Potential Candidates for the Treatment of Type-2 Diabetes. *Phytochem. Rev.* **2022**, *21*, 1049–1079. DOI: 10.1007/s11101-021-09773-1.
[16] Proença, C.; Freitas, M.; Ribeiro, D.; Tomé, S. M.; Oliveira, E. F. T.; Viegas, M. F.; Araújo, A. N.; Ramos, M. J.; Silva, A. M. S.; Fernandes, P. A.; Fernandes, E. Evaluation of a Flavonoids Library for Inhibition of Pancreatic α-Amylase towards a Structure–Activity Relationship. *J. Enzyme Inhib. Med. Chem.* **2019**, *34*, 577–588. DOI: 10.1080/14756366.2018.1558221.
[17] Proença, C.; Freitas, M.; Ribeiro, D.; Oliveira, E. F. T.; Sousa, J. L. C.; Tomé, S. M.; Ramos, M. J.; Silva, A. M. S.; Fernandes, P. A.; Fernandes, E. α-Glucosidase Inhibition by Flavonoids: An in Vitro and *in Silico* Structure–Activity Relationship Study. *J. Enzyme Inhib. Med. Chem.* **2017**, *32*, 1216–1228. DOI: 10.1080/14756366.2017.1368503.
[18] Bagi, P.; Herbay, R.; Varga, B.; Fersch, D.; Fogassy, E.; Keglevich, G. The Preparation and Application of Optically Active Organophosphorus Compounds. *Phosphorus Sulfur Silicon Relat. Elem* **2019**, *194*, 591–594. DOI: 10.1080/10426507.2018.1547725.
[19] Basha, S. T.; Sudhamani, H.; Rasheed, S.; Venkateswarlu, N.; Vijaya, T.; Raju, C. N. Microwave-Assisted Neat Synthesis of α-Aminophosphonate/Phosphinate Derivatives of 2-(2-Aminophenyl) Benzothiazole as Potent Antimicrobial and Antioxidant Agents. *Phosphorus, Sulfur Silicon Relat. Elem.* **2016**, *191*, 1339–1343.
[20] Shameem, M. A.; Orthaber, A. Organophosphorus Compounds in Organic Electronics. *Chemistry* **2016**, *22*, 10718–10735. DOI: 10.1002/chem.201600005.
[21] Jean-Luc, M. Phosphinate Chemistry in the 21st Century: A Viable Alternative to the Use of Phosphorus Trichloride in Organophosphorus Synthesis. *Acc. Chem. Res* **2014**, *47*, 77–87.
[22] Orsini, F.; Sello, G.; Sisti, M. Aminophosphonic Acids and Derivatives. Synthesis and Biological Applications. *Curr. Med. Chem.* **2010**, *17*, 264–289. DOI: 10.2174/092986710790149729.
[23] Mucha, A.; Kafarski, P.; Berlicki, Ł. Remarkable Potential of the α-Aminophosphonate/Phosphinate Structural Motif in Medicinal Chemistry. *J. Med. Chem.* **2011**, *54*, 5955–5980. DOI: 10.1021/jm200587f.
[24] Dhawan, B.; Redmore, D. Optically Active 1-Aminoalkylphosphonic Acids. *Phosphorus, Sulfur, & Silicon & the Related Elements* **1987**, *32*, 119–144. DOI: 10.1080/03086648708074270.
[25] Naydenova, E. D.; Todorov, P. T.; Troev, K. D. Recent Synthesis of Aminophosphonicacids as Potential Biological Importance. *Amino Acids.* **2010**, *38*, 23–30. DOI: 10.1007/s00726-009-0254-7.
[26] Bhattacharya, A. K.; Raut, D. S.; Rana, K. C.; Polanki, I. K.; Khan, M. S.; Iram, S. E. Diversity-Oriented Synthesis of α-Aminophosphonates: A New Class of Potential Anticancer Agents. *Eur. J. Med. Chem.* **2013**, *66*, 146–152. DOI: 10.1016/j.ejmech.2013.05.036.
[27] Huang, X. C.; Wang, M.; Pan, Y. M.; Yao, G. Y.; Wang, H. S.; Tian, X. Y.; Qin, J. K.; Zhang, Y. Synthesis and Antitumor Activities of Novel Thiourea α-Aminophosphonates from Dehydroabietic Acid. *Eur. J. Med. Chem.* **2013**, *69*, 508–520. DOI: 10.1016/j.ejmech.2013.08.055.
[28] Kafarski, P.; Lejczak, B. Aminophosphonic Acids of Potential Medical Importance. *Curr. Med. Chem. Anticancer. Agents.* **2001**, *1*, 301–312. DOI: 10.2174/1568011013354543.
[29] Damiche, R.; Chafaa, S. Synthesis of New Bioactive Aminophosphonates and Study of Their Antioxidant, anti-Inflammatory and Antibacterial Activities as Well the Assessment of Their Toxicological Activity. *J. Mol. Struct.* **2017**, *1130*, 1009–1017. DOI: 10.1016/j.molstruc.2016.10.054.
[30] Sujatha, B.; Mohan, S.; Subramanyam, C.; Prasada Rao, K. Microwave-Assisted Synthesis and anti-Inflammatory Activity Evaluation of Some Novel α-Aminophosphonates. *Phosphorus, Sulfur Silicon Relat. Elem.* **2017**, *192*, 1110–1113.

[31] Kuemin, M.; Donk, W. A. Structure-Activity Relationships of the Phosphonate Antibiotic Dehydrophos. *Chem. Commun. (Camb)* **2010**, *46*, 7694–7696. DOI: 10.1039/c0cc02958k.

[32] Subramanyam, C.; Thaslim Basha, S.; Madhava, G.; Nayab Rasool, S.; Adam, S.; Durga Srinivasa Murthy, S.; Naga Raju, C. Synthesis, Spectral Characterization and Bioactivity Evaluation of Novel α-Aminophosphonates. *Phosphorus, Sulfur. Silicon Relat. Elem.* **2017**, *192*, 267–270. DOI: 10.1080/10426507.2016.1225056.

[33] Sarapuk, J.; Bonarska, D.; Kleszczyńska, H. Biological Activity of Binary Mixtures of 2,4-D with Some Aminophosphonates. *J. Appl. Biomed.* **2003**, *1*, 169–173. DOI: 10.32725/jab.2003.031.

[34] Yang, S.; Gao, X.; Diao, C.; Song, B.; Jin, L.; Xu, G.; Zhang, G.; Wang, W.; Hu, D.; Xue, W.; et al. Synthesis and Antifungal Activity of Novel Chiral α-Aminophosphonates Containing Fluorine Moiety. *Chin. J. Chem.* **2006**, *24*, 1581–1588. DOI: 10.1002/cjoc.200690296.

[35] Herczegh, P.; Buxton, T. B.; McPherson, J. C.; Kovács-Kulyassa, A.; Brewer, P. D.; Sztaricskai, F.; Stroebel, G. G.; Plowman, K. M.; Farcasiu, D.; Hartmann, J. F. Osteo Adsorptive Bisphosphonate Derivatives of Fluoroquinolone Antibacterials. *J. Med. Chem.* **2002**, *45*, 2338–2341. DOI: 10.1021/jm0105326.

[36] Berlicki, L.; Kafarski, P. Computer-Aided Analysis and Design of Phosphonic and Phosphinic Enzyme Inhibitors as Potential Drugs and Agrochemicals. *COC.* **2005**, *9*, 1829–1850. DOI: 10.2174/138527205774913088.

[37] Maheshwara Reddy, N.; Poojith, N.; Mohan, G.; Mohan Reddy, Y.; Saritha, V. K.; Visweswara Rao, P.; Vijaya Kumar Reddy, A.; Swetha, V.; Grigory, V. Z.; Satheesh Krishna, B.; Suresh Reddy, C. Green Synthesis, Antioxidant, and Plant Growth Regulatory Activities of Novel α-Furfuryl-2-Alkylaminophosphonates. *ACS Omega* **2021**, *6*, 2934–2948.

[38] Mohan, G.; Santhisudha, S.; Madhu Kumar Reddy, K.; Vasudeva Reddy, N.; Vijaya, T.; Suresh Reddy, C. Phosphosulfonic Acid-Catalyzed Green Synthesis and Bioassay of α-Aryl-α′-1,3,4-Thiadiazolyl Aminophosphonates. *Heteroat. Chem.* **2016**, *27*, 1–10.

[39] Miller, D. J.; Hammond, S. M.; Anderluzzi, D.; Bugg, T. D. H. Aminoalkylphosphinate Inhibitors of D-Ala-D-Ala Adding Enzyme. *J. Chem. Soc. Perkin Trans. 1* **1998**, *1*, 131–142. DOI: 10.1039/a704097k.

[40] Kuznetsov, Y. I.; Kazanskaya, G. Y.; Tsirulnikova, N. V. Aminophosphonate Corrosion Inhibitors for Steel. *Prot. Met.* **2003**, *39*, 120–123. DOI: 10.1023/A:1022986625711.

[41] Xie, D.; Zhang, A.; Liu, D.; Yin, L.; Wan, J.; Zeng, S.; Hu, D. Synthesis and Antiviral Activity of Novel α-Aminophosphonates Containing 6-Fluorobenzothiazole Moiety. *Phosphorus, Sulfur. Silicon Relat. Elem.* **2017**, *192*, 1061–1067. DOI: 10.1080/10426507.2017.1323895.

[42] Subramanyam, C.; Kiran Kumar, K.; Venkata Ramana, K.; Gladis Raja Malar, C.; Mohan, S.; Mohan, S.; Nagalakshmi, V. Ultrasound Mediated Nano ZnO Catalyzed Synthesis of New α-Aminophosphonates as Potential anti-Diabetic Agents; an *in Silico* ADMET, Molecular Docking Study, α-Amylase and α-Glucosidase Inhibitory Activity. Synth. *Commun* **2023**, *53*, 2041–2060. DOI: 10.1080/00397911.2023.2269583.

[43] Madhu Kumar Reddy, K.; Peddanna, K.; Varalakshmi, M.; Bakthavatchala Reddy, N.; Sravya, G.; Grigory, V. Z.; Suresh Reddy, C. Ceric Ammonium Nitrate (CAN) Catalyzed Synthesis and α-Glucosidase Activity of Some Novel Tetrahydropyridine Phosphonate Derivatives. *Phosphorus, Sulfur. Silicon Relat. Elem.* **2019**, *194*, 812–819. DOI: 10.1080/10426507.2018.1550641.

[44] Murali, S.; Venkataramaiah, C.; Saichaithanya, N.; Mohan, G.; Yasmin, S. H.; Rajendra, W.; Cirandur, S. R. Green Synthesis, Molecular Docking, anti-Oxidant and anti-Inflammatory Activities of α-Aminophosphonates. *Med. Chem. Res.* **2019**, *28*, 1740–1754.

[45] Sreelakshmi, P.; Nadiveedhi, M. R.; Santhisudha, S.; Mohan, G.; Saichaithanya, N.; Sadik, M.; Peddanna, K.; Cirandur, S. R. Nano Sb2O3 Catalyzed Green Synthesis, Cytotoxic Activity, and Molecular Docking Study of Novel α-Aminophosphonates. *Med. Chem. Res.* **2019**, *28*, 528–544.

[46] Mohan, G.; Kuma, S.; Sudileti, M.; Sridevi, C.; Venkatesu, P.; Reddy, C. S. Excellency of Pyrimidinyl Moieties Containing α-Aminophosphonates over Benzthiazolyl Moieties for Thermal and Structural Stability of Stem Bromelain. *Int. J. Biol. Macromol.* **2020**, *165*, 2010–2021. DOI: 10.1016/j.ijbiomac.2020.10.065.

[47] Reddy, K. M. K.; Santhisudha, S.; Mohan, G.; Peddanna, K.; Rao, C. A.; Reddy, C. S. Nano Gd2O3 Catalyzed Synthesis and anti-Oxidant Activity of New α-Aminophosphonates. *Phosphorus, Sulfur. Silicon Relat. Elem.* **2016**, *191*, 933–938. DOI: 10.1080/10426507.2015.1119139.
[48] Ordóñez, M.; Rojas-Cabrera, H.; Cativiela, C. An Overview of Stereoselective Synthesis of α-Aminophosphonic Acids and Derivatives. *Tetrahedron* **2009**, *65*, 17–49. DOI: 10.1016/j.tet.2008.09.083.
[49] Vora, J.; Patel, S.; Sinha, S. Advances in Molecular Docking as a Tool for Drug Discovery and Development. *Front. Pharmacol.* **2019**, *10*, 127.
[50] Altaff, S. K. M.; Raja Rajeswari, T.; Subramanyam, C. Synthesis, α-Amylase Inhibitory Activity Evaluation and *in Silico* Molecular Docking Study of Some New Phosphoramidates Containing Heterocyclic Ring. *Phosphorus, Sulfur. Silicon Relat. Elem.* **2021**, *196*, 389–397. DOI: 10.1080/10426507.2020.1845679.
[51] Pavan Phani Kumar, M.; Anuradha, V.; Subramanyam, C.; Hari Babu, V. V. *In Silico* Molecular Docking Study, Synthesis and α-Amylase Inhibitory Activity Evaluation of Phosphorylated Derivatives of Purine. *Phosphorus, Sulfur. Silicon Relat. Elem.* **2021**, *196*, 1010–1017. DOI: 10.1080/10426507.2021.1960833.
[52] Hanumantha Rao, A.; Madhava Rao, V.; Subramanyam, C.; Priyadarshini, P.; Someswara Rao, S.; Visweswara Rao, P. An *in Silico* ADMET, Molecular Docking Study and Microwave-Assisted Synthesis of New Phosphorylated Derivatives of Thiazolidinedione as Potential anti-Diabetic Agents. *Synth. Commun.* **2022**, *52*, 300–315.
[53] Sujatha, B.; Subramanyam, C.; Venkataramaiah, C.; Rajendra, W.; Prasada Rao, K. Synthesis and anti-Diabetic Activity Evaluation of Phosphonates Containing Thiazolidinedione Moiety. *Phosphorus, Sulfur. Silicon Relat. Elem.* **2020**, *195*, 586–591. DOI: 10.1080/10426507.2020.1737061.
[54] Vijay, M. P.; Kalpana, N. T.; Neha, M. U.; Ramaa, C. S. Synthesis, In-Vitro Evaluation and Molecular Docking Study of N-Substituted Thiazolidinediones as α-Glucosidase Inhibitors. *Chemistry Select* **2022**, *7*, 1–11.
[55] Ramandeep, K.; Rajnish, K.; Nilambra, D.; Ashok, K.; Ashok Kumar, Y.; Manoj, K. Synthesis and Studies of Thiazolidinedione-Isatin Hybrids as α-Glucosidase Inhibitors for Management of Diabetes. *Future Med. Chem.* **2021**, *13*, 1–5.
[56] Wang, G.; Peng, Y.; Xie, Z.; Wang, J.; Chen, M. Synthesis, α-Glucosidase Inhibition and Molecular Docking Studies of Novel Thiazolidine-2,4-Dione or Rhodanine Derivatives. *Med. Chem. Commun.* **2017**, *8*, 1477–1484. DOI: 10.1039/c7md00173h.
[57] Hidalgo-Figueroa, S.; Ramírez-Espinosa, J. J.; Estrada-Soto, S.; Almanza-Pérez, J. C.; Román-Ramos, R.; Alarcón-Aguilar, F. J.; Hernández-Rosado, J. V.; Moreno-Díaz, H.; Díaz-Coutiño, D.; Navarrete-Vázquez, G.; et al. Discovery of Thiazolidine-2,4-Dione/Biphenylcarbonitrile Hybrid as Dual PPAR α/γ Modulator with Antidiabetic Effect: in Vitro, *in Silico* and in Vivo Approaches. *Chem. Biol. Drug Des.* **2013**, *81*, 474–483. DOI: 10.1111/cbdd.12102.
[58] Kaur, J.; Singh, A.; Singh, G.; Verma, R. K.; Mall, R. Novel Indolyl Linked Para-Substituted Benzylidene-Based Phenyl Containing Thiazolidienediones and Their Analogs as α-Glucosidase Inhibitors: synthesis, in Vitro, and Molecular Docking Studies. *Med. Chem. Res.* **2018**, *27*, 903–914. DOI: 10.1007/s00044-017-2112-6.
[59] Senthil Kumar, N.; Vijaya Kumar, V.; Sarveswari, S.; Sarveshwari, G. A.; Gayathri, M. Synthesis of New Thiazolidine-2,4-Dione-Azole Derivatives and Evaluation of Their α-Amylase and α-Glucosidase Inhibitory Activity. *Iran. J. Sci. Technol. Trans. Sci.* **2019**, *43*, 735–745.
[60] Ravikumar, D.; Mohan, S.; Subramanyam, C.; Prasada Rao, K. Solvent-Free Sonochemical Kabachnic-Fields Reaction To Synthesize Some New α-Aminophosphonates Catalyzed By Nano-BF3 SiO2, *Phosphorus. Sulfur Silicon Relat. Elem.* **2018**, *193*, 400–407.
[61] Haji Basha, M.; Subramanyam, C.; Prasada Rao, K. Ultrasound-Promoted Solvent-Free Synthesis of Some New α-Aminophosphonates as Potential Antioxidants. *Main Group Met. Chem.* **2020**, *43*, 147–153. DOI: 10.1515/mgmc-2020-0018.
[62] Madhu Kumar Reddy, K.; Mohan, G.; Bakthavatchala Reddy, N.; Sravya, G.; Peddanna, K.; Grigory, V. Z.; Sridevi, C.; Suresh Reddy, C. Synthesis, Antioxidant Activity, and α-Glucosidase Enzyme Inhibition of *α*-Aminophosphonate Derivatives Bearing Piperazine-1,2,3-Triazole Moiety. *J. Heterocycl. Chem.* **2021**, *58*, 172–181.

[63] Priyadarsini, P.; Madhava Rao, V.; Hanumatha Rao, A.; Subramanyam Ch, R. Y. A Simple, Efficient Synthesis and Molecular Docking Studies of 2-Styrylchromones. *Org. Commun.* **2021**, *14*, 121–132.
[64] Haji Basha, M.; Subramanyam, C.; Gladis Raja Malar, C.; Someswara Rao, S.; Prasada Rao, K. Nano $TiO_2.SiO_2$ Catalyzed, Microwave Assisted Synthesis of New *α*-Aminophosphonates as Potential anti-Diabetic Agents: *In Silico* ADMET and Molecular Docking Study. *Org. Commun.* **2022**, *15*, 167–183.
[65] Terry, R. S.; James, R. K.; Stephen, R. J.; Xue-Qing, C.; Arthur, D.; Yi, Li *In Silico* ADME/Tox: Why Models Fail. *J Comput. Aid. Mol. Des.* **2003**, *17*, 83–92.
[66] Tingjun, H.; Junmei, W.; Wei, Z.; Xiaojie, X. ADME Evaluation in Drug Discovery. 6. Can Oral Bioavailability in Humans Be Effectively Predicted by Simple Molecular Property-Based Rules? *J. Chem. Inf. Model* **2007**, *47*, 460–463.
[67] Trudy, R.; David, L. Physiologically Based Pharmacokinetic Modeling 1: Predicting the Tissue Distribution of Moderate-to-Strong Bases. *J. Pharm. Sci.* **2005**, *94*, 1259–1276.
[68] Daina, A.; Zoete, V. A Boiled-Egg to Predict Gastrointestinal Absorption and Brain Penetration of Small Molecules. *Chem. Med. Chem.* **2016**, *11*, 1117–1121. DOI: 10.1002/cmdc.201600182.
[69] Montanari, F.; Ecker, G. F. Prediction of drug-ABC-Transporter Interaction-Recent Advances and Future Challenges. *Adv. Drug Deliv. Rev.* **2015**, *86*, 17–26. DOI: 10.1016/j.addr.2015.03.001.
[70] Hollenberg, P. F. Characteristics and Common Properties of Inhibitors, Inducers, and Activators of CYP Enzymes. *Drug Metab. Rev.* **2002**, *34*, 17–35. DOI: 10.1081/dmr-120001387.
[71] Shiew-Mei, H.; John, M. S.; Lei, Z.; Kellie, S. R.; Srikanth, N.; Robert, T.; et al. New Era in Drug Interaction Evaluation: US Food and Drug Administration Update on CYP Enzymes, Transporters, and the Guidance Process. *J. Clin. Pharmacol.* **2008**, *48*, 662–670.
[72] Potts, R. O.; Guy, R. H. Predicting Skin Permeability. *Pharm. Res.* **1992**, *9*, 663–669. DOI: 10.1023/a:1015810312465.
[73] Lipinski, C. A.; Lombardo, F.; Dominy, B. W.; Feeney, P. J. Experimental and Computational Approaches to Estimate Solubility and Permeability in Drug Discovery and Development Settings. *Adv. Drug Del. Rev.* **2001**, *46*, 3–26.
[74] Ghose, A. K.; Viswanadhan, V. N.; Wendoloski, J. J. Prediction of Hydrophobic (Lipophilic) Properties of Small Organic Molecules Using Fragmental Methods: An Analysis of ALOGP and CLOGP Methods. *J. Phys. Chem. A* **1998**, *102*, 3762–3772. DOI: 10.1021/jp980230o.
[75] Veber, D. F.; Johnson, S. R.; Cheng, H. Y.; Smith, B. R.; Ward, K. W.; Kopple, K. D. Molecular Properties That Influence the Oral Bioavailability of Drug Candidates. *J. Med. Chem.* **2002**, *45*, 2615–2623. DOI: 10.1021/jm020017n.
[76] Egan, W. J.; Lauri, G. Prediction of Intestinal Permeability. *Adv. Drug Deliv. Rev.* **2002**, *54*, 273–289. DOI: 10.1016/s0169-409x(02)00004-2.
[77] Muegge, I.; Heald, S. L.; Brittelli, D. Simple Selection Criteria for Drug-like Chemical Matter. *J. Med. Chem.* **2001**, *44*, 1841–1846. DOI: 10.1021/jm015507e.
[78] Trott, O.; Olson, A. J. Auto Dock Vina: improving the Speed and Accuracy of Docking with a New Scoring Function, Efficient Optimization and Multithreading. *J. Comput. Chem.* **2010**, *31*, 455–461. DOI: 10.1002/jcc.21334.
[79] Nickavar, B.; Amin, G. Enzyme Assay Guided Isolation of an Alpha-Amylase Inhibitor Flavonoid from Vaccinium Arctostaphylos Leaves. *Iran. J. Pharm. Res.* **2011**, *10*, 849–853.
[80] Patil, V. S.; Nandre, K. P.; Ghosh, S.; Rao, V. J.; Chopade, B. A.; Sridhar, B.; Bhosale, S. V.; Bhosale, S. V. Synthesis, Crystal Structure and anti-Diabetic Activity of Substituted (E)-3-(Benzo[d]Thiazol-2-Ylamino)Phenylprop-2-en-1-One. *Eur. J. Med. Chem.* **2013**, *59*, 304–309.
[81] Kim, J. S.; Hyun, T. K.; Kim, M. J. The Inhibitory Effects of Ethanol Extracts from Sorghum, Foxtail Millet and Proso Millet on α-Glucosidase and α-Amylase Activities. *Food Chem.* **2011**, *124*, 1647–1651. DOI: 10.1016/j.foodchem.2010.08.020.